Microporous and Mesoporous Materials 123 (2009) 177–184

Contents lists available at ScienceDirect

Microporous and Mesoporous Materials

journal homepage: www.elsevier.com/locate/micromeso

Synthesis of mesostructured ferric oxyhydroxides templated by alkyl surfactants: Effect of pH, F^- and solvents, and their adsorption isotherms for As(V)

Feihu Li [a,b], Hao Fu [a], Jianping Zhai [a], Qin Li [a,*]

[a] State Key Laboratory of Pollution Control and Resource Reuse, School of the Environment, Nanjing University, Nanjing 210093, China
[b] School of Environmental Science and Engineering, Nanjing University of Information Science and Technology, Nanjing 210044, China

ARTICLE INFO

Article history:
Received 25 January 2009
Received in revised form 30 March 2009
Accepted 31 March 2009
Available online 5 April 2009

Keywords:
Mesostructured ferric oxyhydroxides
CTAB
SDS
Arsenic
Adsorption

ABSTRACT

Mesostructured ferric oxyhydroxides (MFOs) were synthesized using both cetyltrimethylammonium bromide (CTAB) and sodium dodecylsulfonate (SDS) as templates in the present study. For CTAB-templating route, the effect of pH and fluoride ions on the resulting MFOs has been evaluated, and the active role of fluoride ions in promotion the mesostructural ordering was verified. Besides, the effect of solvents and hydrolysis ratio on the synthetic layered MFOs was examined via SDS-templating route. X-ray diffraction (XRD), transmission electron microscopy (TEM), and nitrogen physisorption were employed to characterize the MFOs before two typical MFOs with surface areas of 144.7 and 88.1 $m^2 g^{-1}$, respectively, were evaluated as potential adsorbent for As(V) removal. Both MFOs presented adsorption isotherms well fitting the Freundlich equation. The two MFOs exhibited adsorption capacities of 75.19 and 10.68 mg g^{-1}, respectively, and could be adopted as adsorbent for As(V) removal.

© 2009 Elsevier Inc. All rights reserved.

1. Introduction

Arsenic contamination in global aqueous systems, especially in Bangladesh [1–3], India [4,5], Vietnam [6], Taiwan [7], Argentina [8], the Western US [9], and China [10,11], is still a great challenge for drinking water supplies, subsequently posing a risk to human health. In addition, the recent reduction in the maximum contaminant level (MCL) for arsenic in drinking water from 0.050 to 0.010 mg L^{-1} as regulated by the world health organization (WHO), will be accepted and adopted as the drinking water standard by more and more countries [12]. The tightening of arsenic standard will consequently impact the on-the-run technology applications for drinking water treatments, and could result in lower treatment goals for remediation of arsenic-contaminated sites. Certainly, current and future drinking water and groundwater treatment systems will require better-performing technologies, either improved or newly developed, to achieve this lower level [13].

Of various well-reputed technologies for arsenic removal, adsorption has received more attention due to its high removal efficiency, especially without yielding hazardous byproducts [14,15]. Because of the Fe(III)'s special affinity toward inorganic arsenic species and consequent selectivity in the adsorption process, Fe(III)-based materials including goethite [16], hematite [17], ferrihydrite [18], iron-oxide-coated sand [19], Fe(III)-loaded cellulose sponge [20], iron-containing mesoporous carbon [21], hydrous ferric oxides (HFOs) [22] are the most used adsorbents. Hydrous ferric oxides/oxyhydroxides traditionally used in arsenic removal were usually, however, limited by lower efficiency in intraparticle diffusion for their lower surface area as compared to Fe(III)-loaded adsorbents with higher surface area [23].

On the other hand, the recent successes in synthesis of mesoporous materials, especially in synthesis of mesostructured transition-metal oxides/oxyhydroxides templated by alkyl surfactants in thermal solution [24,25], make it very promising to prepare mesostructured ferric oxyhydroxides (MFOs) for arsenic removal from aqueous systems. To date, many types of mesostructured ferric oxides have been reported using cetyltrimethylammonium bromide (CTAB) [26–28], sodium dodecylsulfonate (SDS) [29,30], and neutral alkyl amine [31,32] as templates. Only lamellar/layered mesostructured ferric oxyhydroxides, however, were synthesized via the well-known S^-I^+ pathway in the absence of halide ions such as chloride ions (Cl^-) and fluoride ions (F^-) [33–35]. Generally, fluoride ions were usually used as catalyst in synthesis of zeolite, and additionally, it has been proved that F^- were also efficient in generation of well-defined ordered mesoporous silica [36]. Are they still efficient in synthesis of mesoporous transition-metal oxides/oxyhydroxides, especially MFOs when using CTAB as template? Little works has been reported on these so far, even though the well-known F^--mediating pathway (i.e., $S^+F^-I^+$) to mesoporous materials has been established and accepted for more than one decade [24]. For the aforementioned S^-I^+ pathway, the effect of aliphatic alcohols on the final mesostructure of

* Corresponding author. Tel./fax: +86 25 8359 2903.
E-mail addresses: jpzhai@nju.edu.cn, favorlee@163.com (Q. Li).

1387-1811/$ - see front matter © 2009 Elsevier Inc. All rights reserved.
doi:10.1016/j.micromeso.2009.03.044

mesostructured ferric oxides has been examined using sodium hexadecylsulfonate as template [37]. The effect of alcohols especially ethanol (EtOH) on synthesis of ferric oxyhydroxides templated by SDS, however, has remained unevaluated until now.

Herein, we report the synthesis of MFOs with worm-like pores using CTAB as template in the presence of F^-, and demonstrate the active role of F^- in promotion the mesostructural ordering of mesostructured transition-metal oxides, specifically MFOs for the first time. Aside from effect of F^- concentration, the effect of pH on the resulting MFOs has also been examined in the CTAB-templating route. Whereas, in the SDS-templating pathway, the effect of alcohols especially ethanol as well as hydrolysis ratio (defined as the molar ratio of hydroxy ions to ferric ions in the synthetic solution) has been investigated. The resulting MFOs were then characterized by XRD, TEM, and nitrogen physisorption. Finally, two typical MFOs selected were evaluated as adsorbents for As(V) removal from aqueous solution.

2. Experimental section

2.1. Mesostructured ferric oxyhydroxides templated by CTAB

Mesostructured ferric oxyhydroxides templated by CTAB were synthesized using ferric nitrate as ferric source. In a typical synthesis, 6 mmol of $Fe(NO_3)_3 \cdot 9H_2O$ was dissolved in 25 mL of ethanol at room temperature by magnetic stirring to form a yellow solution, then a solution of 6 mmol of CTAB in 30 mL of double distilled water was added with strongly stirring until a homogenous solution was achieved. The solution was then made basic by dropwise adding different amount of NH_4OH (~25 wt.%) and pH was adjusted to a desired value before transferring to a sealed Teflon-lined stainless vessel (100 mL) and ageing in a oven at 40 °C for 24 h. After further incubating at 80 °C for 4–6 h and air-cooling to room temperature, the yellow precipitate was recovered by centrifugalizing at 4000 rpm followed by washing with hot alcohol several times to remove the remaining surfactant. Finally, drying of such precipitates at 50 °C for 6–8 h yielded CTAB-templated MFOs.

To exam the effect of pH on the final MFOs, a second hexad of ferric nitrate-surfactant solutions were prepared and the pHs were adjusted, by varying the amount of NH_4OH dropwise added, to 3.5, 5.5, 7.0, 8.5, 10.0, and 10.7, respectively. Another second hexad of ferric nitrate-surfactant solutions were also prepared to evaluate the effect of F^- on the resulting MFOs. The hexad solutions were averaged into two groups, 1 and 2. Three mmol of NH_4F were introduced to each one of group 1 to ensure the F^-/Fe^{3+} (mol/mol) = 0.5 and the pH were adjusted to 3.5, 5.5, and 10.7 respectively. Group 2 samples were added by 6 mmol of NH_4F (F^-/Fe^{3+} = 1.0) and pH were also adjusted to 3.5, 5.5, and 10.7 respectively.

2.2. Mesostructured ferric oxyhydroxides templated by SDS

An orthogonal design method was used to investigate the effects of solvents used, hydrolysis ratio r (defined as OH^-/Fe^{3+} molar ratio of the synthetic solution) and the ageing time on the resulting SDS-templated MFOs. In detail, the following procedures are adopted: a ennead of 6 mmol of $FeCl_3$ were dissolved in three triples of 10 mL of 0, 0.3, and 0.9 M NaOH solutions and pre-hydrolysis for 30–60 min to yield three triads of ferric solutions with hydrolysis ratio r = 0, 0.5, and 1.5, respectively. Another ennead of 12 mmol of SDS were dissolved in 40 mL of solvents (i.e., DD H_2O, EtOH, and propanol (PrOH)) at elevated temperature to form three triads of SDS-solvent solutions before being dropwise added by the three triads of ferric solutions with simultaneously stirring and ultrasonicating for 30 min. A follow-up 60-min stirring at 40 °C is necessary to ensure that all the reagents are homogeneously dispersed in the solution. Then, the solution was transferred into a sealed Teflon-lined stainless vessel (100 mL) and aged in an oven at 80 °C for 24 h. After air-cooling to ambient temperature, the complexes were filtered by suction and washed repeatedly with excessive hot alcohol to extract the remaining SDS followed by air-drying to yield the SDS-templated MFOs. Selected as-synthesized MFO sample (solvent = H_2O, r = 0) was calcined at 400 °C for 6 h to investigate the effect of calcination on the final MFO.

2.3. Materials characterization

X-ray diffraction (XRD) analysis was conducted using an ARL X'TRA diffractometer at a voltage of 40 kV and a current of 40 mA with Cu-Kα radiation. For small-angle (typically 1–10°) diffraction, a scanning step size of 0.02° with a scanning rate of 2° per min was adopted, while a scanning step size of 0.02° with a scanning rate of 5° per min was used in wide-angle (herein 10–50°) diffraction. Transmission electron microscopy (TEM) images and the electron diffraction (ED) patterns were recorded on a JEOL JEM-200CX microscope at an accelerating voltage of 200 kV. The samples were dispersed in absolute alcohol and ultrasonicated for 5–10 min prior to TEM recording.

Surface area, pore volume and pore size distribution of selected MFOs were measured by nitrogen physisorption at 77 K with a Micromeritics ASAP 2010 apparatus. Before adsorption analysis, MFO samples were degassed at 353 K under vacuum for 12 h. The Brunauer–Emmett–Teller (BET) method was used to calculate the surface areas using the adsorption data, whereas the Barrett–Joyner–Halenda (BJH) algorithm was adopted to estimate the pore size distribution from the adsorption branch of the isotherm. The total pore volume was evaluated from the amount of nitrogen adsorbed at a relative pressure of 0.99 [38].

2.4. Arsenate adsorption tests

Two typical MFOs – the CTAB-templated MFO synthesized at pH 5.5 with Fe^{3+}/F^- (mol/mol) = 1 (termed as MFO-C) and the SDS-templated MFO prepared at r = 0.5 using H_2O as solvent (termed as MFO-S), were selected as adsorbent for arsenate in aqueous solution. In a typical adsorption test, 100 mg of adsorbent was added separately to a conical flask (250 mL) before 100 mL of As(V) solution with given concentration, pH (=7.0 ± 0.1) and ionic strength (I = 0.01 M NaCl) was added. After sealing and premixing on a vortex mixer for 5 min, the mixture was shaken at 180 rpm and 25 °C for approximately 24 h on a reciprocal shaker. Then, it was filtered with a 45 μm membrane filter for analysis. The pH was measured with a pH meter (model 828, Orion, US). As(V) in the supernatant was analyzed on an AFS-610 atomic fluorescence spectrometer (Beijing Rayleigh Analytical Instrument Co., China) following the hydride-generation atomic fluorescence spectrometry (HG-AFS) procedure. The adsorption isotherms were studied by varying concentration of As(V) solution with a fixed dose of adsorbent (i.e., 100 mg). Adsorption isotherms were modeled using both the Langmuir and the Freundlich equations which are expressed as follows (Eqs. (1) and (2)):

$$\text{Langmuir}: q_e = \frac{bq_m C_e}{1 + bC_e} \tag{1}$$

$$\text{Freundlich}: q_e = KC_e^{\frac{1}{n}} \tag{2}$$

where C_e is the equilibrium concentration of As(V) (mg L^{-1}), q_e is the amount adsorbed under equilibrium (mg g^{-1}), q_m (mg g^{-1}) is the theoretical maximum adsorption capacity of the adsorbent for

As(V), and b (L mg^{-1}) is a Langmuir binding constant related to the energy of adsorption, K and n are the Freundlich empirical constants.

3. Results and discussion

3.1. CTAB-templated MFOs

3.1.1. XRD

The XRD patterns of CTAB-templated MFOs as a function of pH in the synthetic solution without fluoride ions were shown in Fig. S1. There were no distinct peaks observed in the small-angle XRD patterns of the resulting MFOs (Fig. S1a), implying no ordered mesopore was formed in the pH range 3.5–10.7 in the absence of fluoride ions. Although mesoporous iron oxides templated by CTAB have been reported using diverse bases as precipitant [26,27], neither of these literature presented XRD patterns with any apparent peaks corresponding to ordered mesopore diffraction. This observation suggests that CTAB is incapable of templating mesopore iron oxides with ordered pore structure. In the case of MFOs, our results depicted here seem to further confirm that CTAB cannot generate ordered MFOs either. As illuminated in Fig. S1b, for MFOs formed in the pH range 3.0–8.5, only a halo (in 2θ range of 30–40°) deriving from the diffuse scattering of X-ray by amorphous iron oxides was observed in their wide-angle XRD patterns, whereas several peaks relating to hematite (α-Fe_2O_3, JCPDS PDF # 33-0664) were appeared in the patterns of MFOs synthesized in solutions with pH $\geqslant$10. However, hydrolysis of ferric nitrate at elevated temperature usually yields goethite or hematite [39], our data seem to indicate that hematite was exclusively formed in the presence of CTAB.

When introducing fluoride ions to the synthetic solution, as shown in Fig. 1a and c, a single diffraction peak, independent of the F^- concentration, appeared in all small-angle XRD patterns of CTAB-templated MFOs. The peak with d spacing of ~83.4 Å seems to be responsible for diffraction of a worm-like structure. Moreover, comparing of the XRD patterns having the same pH in Fig. 1a and c suggests that the diffraction intensity increases with increasing F^- concentration and that the d spacing decreases as the F^- concentration increases. This observation implies that the structural ordering of the resulting MFOs increased with increasing F^- concentration, which in some sense proved the active role of F^- in promotion of the structural ordering of MFOs. The role of F^- in mediating synthesis of MFOs may be achieved through the well-known $S^+F^-I^+$ pathway by Coulomb attraction of ions with opposite charges, i.e., the charge-density matching, which was hackneyed in synthesis of mesoporous silica [24,40]. Although this charge-density matching mechanism for CTAB-templated MFOs in the presence of F^- should be further confirmed, it is nevertheless, the first successful attempt to synthesize worm-like MFOs in the presence of fluoride ions to date.

Likewise, the wide-angle XRD patterns (Fig. 1b and d) varied apparently after introducing F^- to the solution. Despite that the solution pH was as low as 5.5, other two types of peaks relating to akaganeite (β-FeOOH, JCPDS PDF # 34-1266) and goethite (α-FeOOH, JCPDS PDF # 29-07136) arise in the XRD patterns of MFOs as compared to the wide-angle XRD patterns shown in Fig. 1b.

The mineralogical component of the resulting MFOs was pH-dependent and varied obviously from akaganeite and goethite to goethite and hematite in the case of F^-/Fe^{3+} = 0.5, and from akaganeite to akaganeite and goethite and to goethite and hematite in the case of F^-/Fe^{3+} = 1.0 as pH increased form 5.5 to 8.5 and to 10.7, respectively. Although the diffraction peaks of akaganeite were broad and low, indicating the akaganeite was ill-crystallized; introducing F^- to the synthetic solution indeed enables amorphous iron oxides to crystallize at pH as low as 5.5. This observation further confirmed that F^- is an excellent mineralizer in synthesis of crystalline microporous/mesoporous materials. Additionally, a

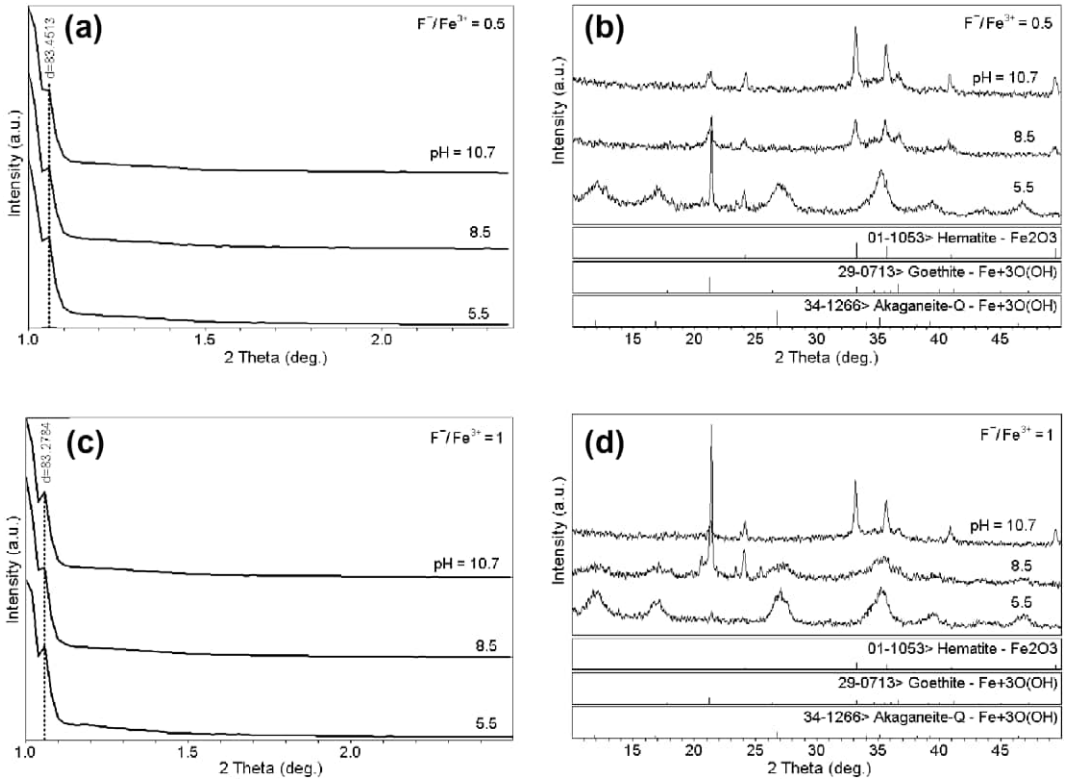

Fig. 1. Small-angle (a, c) and wide-angle (b, d) XRD patterns of the CTAB-templated MFOs as a function of pH at F^-/Fe^{3+} (mol/mol) = 0.5 (a, b), 1.0 (c, d), respectively.

higher concentration of F^- preferentially facilitated the formation of akaganeite other than goethite and hematite at pH 8.5 and 5.5 (see Fig. 1b and d), which is in good agreement with Flynn's results [39].

3.1.2. TEM

The active role of F^- in generation of worm-like mesopore in MFOs was also confirmed by the TEM images (Fig. 2). In the absence of F^- in the synthetic solution, a MFO with loose and floccule-like particle cluster was obtained (Fig. 2a), whereas a MFO with worm-like pore array was yielded in the presence of F^- (Fig. 2b). This observation should be a strong evidence for extending the active range of F^- from synthesis of ordered mesoporous silica to synthesis of mesoporous transition-metal oxyhydroxides, since the presence of F^- resulting in formation of MSU-X-type mesoporous silica with a single reflection and worm-like pore structure has been verified [41]. In addition, the electron diffractogram with diffraction rings, as shown in the inset of Fig. 2b, testified the low-crystalline nature of such MFOs which is consistent with the XRD data (Fig. 1b).

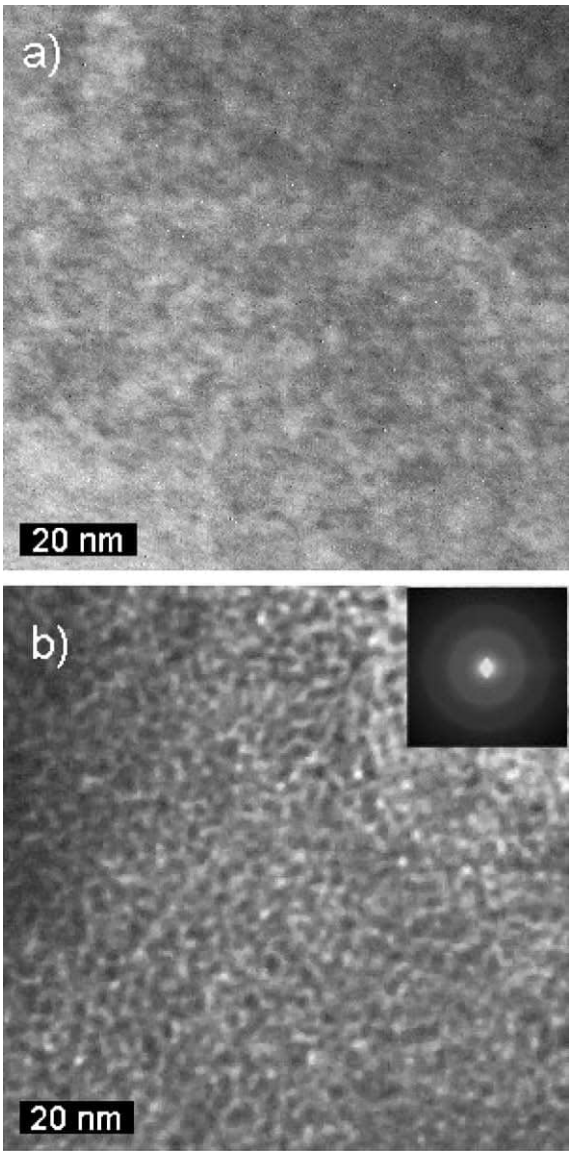

Fig. 2. TEM images of the CTAB-templated MFOs at pH 5.5. (a) Without F^- in the synthetic solution; (b) F^-/Fe^{3+} (mol/mol) = 1.0 (inset is the corresponding electronic diffractogram).

3.1.3. N_2 physisorption

The N_2 physisorption results of MFO sample synthesized at F^-/Fe^{3+} (mol/mol) = 1.0 and pH 5.5 were depicted in Fig. 3. The N_2 adsorption isotherm shows type IV isotherm with a near H1-type hysteresis loop at relative pressure (P/P_0) = 0.5–0.8 connected with an H4-type hysteresis loop at relative pressure (P/P_0) = 0.8–1.0, which is characteristic of mesoporous materials with relatively regular pore along with narrow slit-like pore [42]. The former hysteresis loop may be assigned to worm-like pore yielded via the $S^+F^-I^+$ assembly pathway, whereas the latter should be related to the large interparticle pore of irregular MFOs particles. The MFO exhibits a narrow pore size distribution with an average BJH pore diameter of 18 Å (the inset of Fig. 3). The MFO has a total pore volume of 0.23 $cm^3\ g^{-1}$ and a BET specific surface area of 144.7 $m^2\ g^{-1}$ that is smaller than literature's data [26], this reduction in surface area may be owing to a part of surfactants remaining in the mesopores after alcohol extraction, or more likely, originating from pore structure shrinking promoted by the introduced F^-.

3.2. SDS-templated MFOs

3.2.1. XRD

The XRD patterns of the SDS-templated MFOs as a function of hydrolysis ratio r using H_2O and EtOH as solvent were presented in Fig. 4. For r = 0 and 0.5, the MFOs obtained were lamellar with $d_{(001)}$ spacing of 36.46 Å, $d_{(002)}$ spacing of 18.33 Å, and $d_{(003)}$ spacing of 12.24 Å, respectively (Fig. 4a). These d values are in agreement with data reported in previous literature [34,37], signifying similar lamellar mesostructures were obtained, i.e., these resulting MFOs were mesostructured ferric oxyhydroxide/surfactant hybrid materials other than pure MFOs. When the hydrolysis ratio r was increased to 1.5, a disparate set of diffraction peaks with d spacings of 30.92, 15.39, and 10.26 Å appeared in the small-angle XRD patterns (*cf.* Fig. 4a). These peaks, likewise, could be easily indexed and assigned to (0 0 1), (0 0 2), and (0 0 3) planes of another lamellar MFO with different d spacings.

The dramatic decrease in d spacings when increasing hydrolysis ratio from 0.5 to 1.5 is speculated to cause by the increase in thickness of the layered MFOs wall. Specifically, within the MFOs wall, the building blocks, i.e., iron polycations deriving from the completely hydrolysis of iron salts promoted by OH^- especially at higher r, were relatively lower charged as compared to iron oligomer, e.g., iron monomers, iron dimers from hydrolysis of iron salts at lower r [37]. Another probable reason accounting for the decreas-

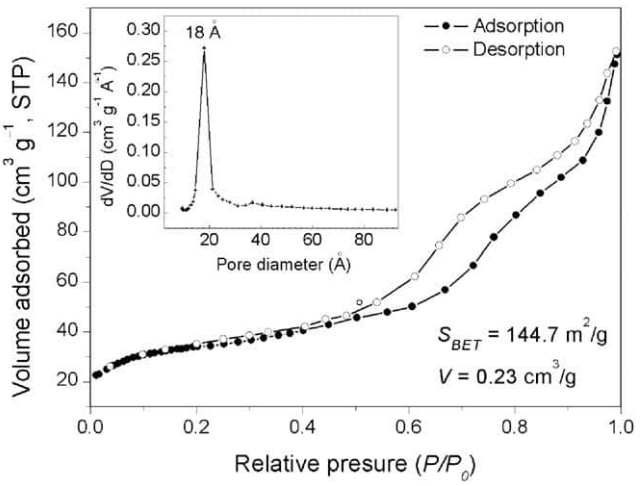

Fig. 3. N_2 adsorption/desorption isotherm of MFO sample synthesized at F^-/Fe^{3+} (mol/mol) = 1.0 and pH 5.5 (inset is the corresponding pore size distribution curve).

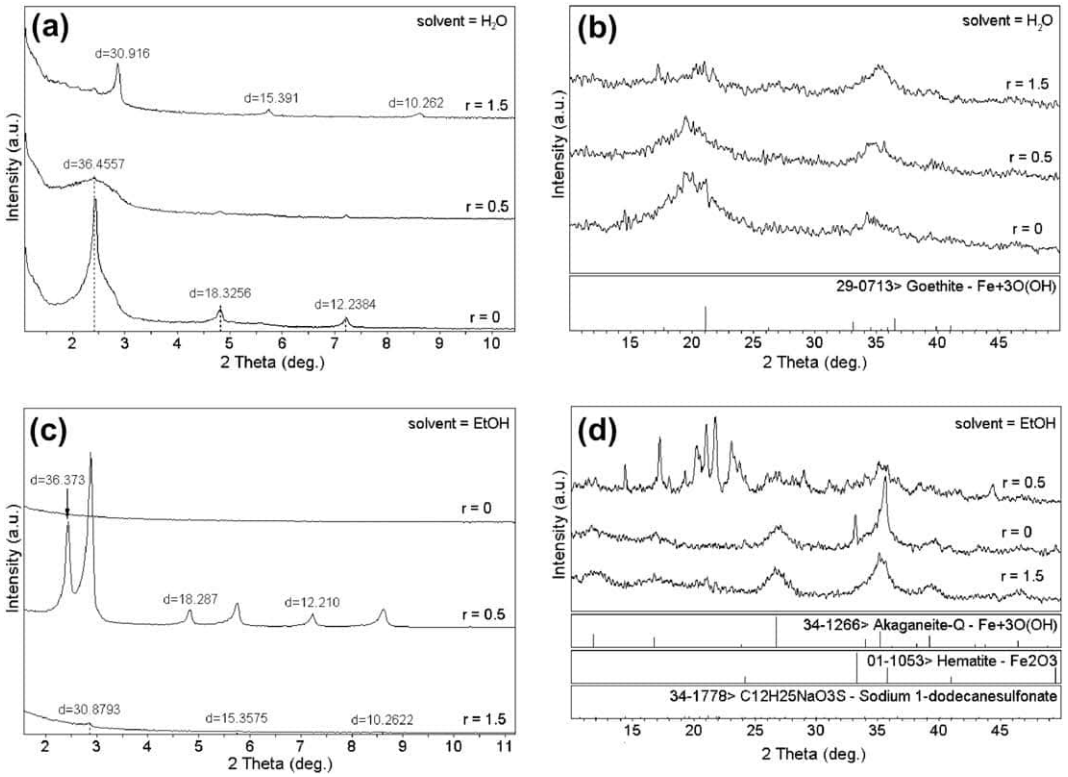

Fig. 4. Small-angle (a, c) and wide-angle (b, d) XRD patterns of the SDS-templated MFOs as a function of hydrolysis ratio *r* using H_2O (a, b) and EtOH (c, d) as solvent, respectively.

ing *d* spacing may be that the alkyl chains of the surfactant (i.e., SDS) that bilayeredly array in the interplane of layered MFOs wall and interdigitate with each other at higher *r* [34], which accordingly resulted in a decrease in *d* spacing. The wide-angle XRD patterns (Fig. 4b) suggested that these MFOs are mainly poor-crystallized goethite in mineralogy. Additionally, the diffraction peaks sharpened and narrowed with increasing *r*, implying higher *r* promoted the formation of MFOs with higher atomic-scale ordering and crystallinity.

Substituting EtOH for H_2O as solvent resulted in disparate XRD patterns (Figs. 4c and d). For $r = 0$, no peaks presented in the small-angle XRD patterns (Fig. 4c) indicating no mesostructure formed, while a set of *d* spacings of 30.88, 15.36, and 10.26 Å assignable to (0 0 1), (0 0 2), and (0 0 3) planes emerged in Fig. 4c as for $r = 1.5$, suggesting a lamellar MFO similar to aforementioned species synthesized at $r = 1.5$ using H_2O as solvent was yielded. Their peak intensities were quite lower than those of the former MFO, implicating the mesostructural ordering of MFO was decreased when using EtOH as solvent. This reduction in mesostructural ordering was probably arisen from the increase in hydrophobicity of SDS surfactant caused by the EtOH solvent according to the well-known geometric model [40]. The small-angle XRD pattern of MFO synthesized at $r = 0.5$ (Fig. 4c) was unexpectedly featured by two sets of peaks. The first set of peaks with *d* spacings of 36.37, 18.28, and 12.21 Å were assigned to (0 0 1), (0 0 2), and (0 0 3) planes of layered MFO/SDS hybrid material [34,35], while the latter with *d* spacings of 30.88, 15.36, and 10.26 Å were more likely related to (0 0 1), (0 0 2), and (0 0 3) planes of pure lamellar MFOs.

Unlike the uniform mineralogical component of MFOs achieved in H_2O solvent with varying *r*, the mineralogical components of MFOs obtained in EtOH solvent varied with diverse hydrolysis ratio (Fig. 4d). As *r* increased from 0 through 0.5 to 1.5, the mineralogical components of the MFOs transformed from a blend of low-crystalline akaganeite (β-FeOOH, JCPDS PDF # 34-1266) and some hematite (α-Fe_2O_3, JCPDS PDF # 01-1053) via a mixture of the low-crystalline akaganeite and the remaining SDS ($C_{12}H_{25}SO_3Na$, JCPDS PDF # 34-1778) to a sole low-crystalline akaganeite.

When using PrOH as solvent, neither lamellar nor other mesostructures with diverse symmetry types were formed at different *r* as indicated by the small-angle XRD pattern (Fig. S2a). This phenomenon could be explained as follows: the chain length of PrOH was greater than that of EtOH, the increase in hydrophobicity of SDS enhanced by the PrOH was consequently greater than that caused by EtOH, causing an effective packing parameter $g > 1$ – the critical value for generation of mesoporous materials [40]. As suggested in Fig. S2b, only low-crystalline akaganeite was obtained at various *r*, which seems to well correlate the hydrophobicity of SDS with the mineralogy of the resulting MFOs. That is, the increase in hydrophobicity of SDS favored the formation of akaganeite other than goethite (*cf.* Fig. 4b and d, and S2b).

Fig. 5 depicts the XRD patterns of typical MFO as a function of template removal approaches. The diffraction peaks of the as-synthesize species were broad and low due to the full-fill of the lamellar mesostructure (Fig. 5a). After extraction the surfactant by excessive hot alcohol, these peaks, corresponding to (0 0 1), (0 0 2), (0 0 3) planes, sharpened with increasing intensity, implying removal of SDS from the mesostructure and an improvement in mesostructural ordering of the MFO (Fig. 5b). As expected, calcination of the MFO at 400 °C led to completely collapse of the lamellar MFO (Fig. 5c), which further suggested that calcination was not suitable for lamellar mesostructure for template removal.

3.2.2. TEM

The TEM images of SDS-templated MFOs synthesized in H_2O- and EtOH-solvent systems at $r = 0.5$ are shown in Fig. 6. For MFOs derived from H_2O-solvent systems, striped TEM images (Fig. 6a) indicative of lamellar mesostructure was observed. The spacing of *ca.* 9 nm between any adjacent stripes was also in good agree-

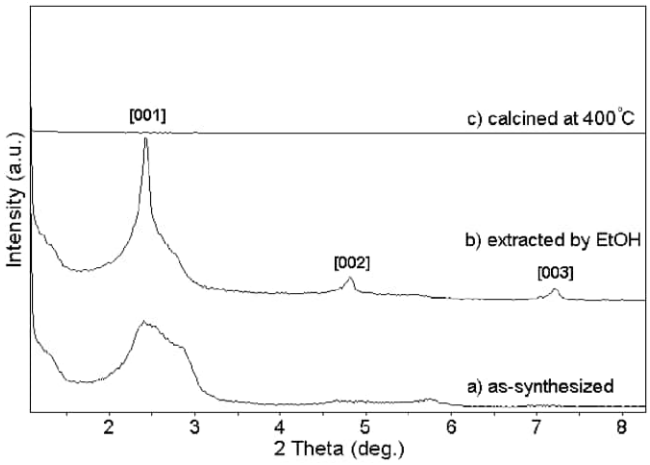

Fig. 5. XRD patterns of the SDS-templated MFO (solvent = H_2O, $r = 0$) as a function of template removal approaches. (a) As-synthesized, (b) extracted by EtOH, (c) calcined at 400 °C.

ment with the d_{004} value of 9.11 nm calculated from XRD data even though the reflection peak relating to (0 0 4) plane was not as sharp and clear as other planes in the XRD pattern (*cf.* Fig. 4a). Similarly, MFOs from EtOH-solvent systems exhibits a layered array of channels with lower ordering and clarity as compared to MFOs from H_2O-solvent systems (*cf.* Figs. 6a and b). More interesting is that several subhexagonal pore arrays as marked with white round dash line appeared in Fig. 4b, which may be involuntarily considered as hexagonal pore arrays, subsequently deducing a 2D hexagonal pore structure. But in the present situation, it is more likely derived from the overlapping of the two different types of lamellar channels as verified by the aforementioned XRD results (Fig. 4c).

3.2.3. N_2 physisorption

The N_2 physisorption data of MFO species from EtOH-solvent system, as shown in Fig. 7, revealed that MFO possesses a type IV adsorption isotherm and an H1-type hysteresis loop at relative pressure (P/P_0) = 0.4–0.7 combined with an H3-type hysteresis loop at relative pressure (P/P_0) = 0.7–1.0. This bi-hysteresis loop indicated coexistence of cylindrical pore mesostructure and layered mesostructure in such MFO. Moreover, it has a BET specific surface area of 88.1 $m^2\,g^{-1}$ and a total pore volume of 0.14 $m^3\,g^{-1}$, quite less than the data as reported in literature [33], suggesting much more template remained in the resulting MFO mesostructure. Its BJH pore diameter (the inset of Fig. 7) was characterized by bimodal distribution – a narrow distribution centred at 25.6 Å (i.e., average BIH pore diameter) along with a relative broad distribution centred at *ca.* 50 Å.

3.3. Adsorption isotherms of As(V) on typical MFOs

Fig. 8 shows the adsorption isotherms of As(V) on selected MFOs, namely the CTAB-templated MFO synthesized at pH 5.5 with Fe^{3+}/F^- (mol/mol) = 1 (termed as MFO-C) and the SDS-templated MFO prepared at $r = 0.5$ using H_2O as solvent (termed as MFO-S). Both the Langmuir and the Freundlich equations (Eqs.(1) and (2)) were used to describe the adsorption isotherms in Fig. 8 and especially, the Langmuir equation was employed to calculate the adsorption capacities – the theoretical maximum adsorption capacity (i.e., q_m). Linear plots of C_e/q_e versus C_e for MFO-C were achieved with regression coefficient (R^2), b (L mg^{-1}), and q_m (mg g^{-1}) of 0.953, 0.25, and 75.19, respectively. Whereas the Freundlich parameters (i.e., R^2, n, and K) obtained by linear plotting of lnq_e versus lnC_e were 0.997, 2.76, and 15.92, respectively, indicating that adsorption of As(V) onto MFO-C follows the Freundlich isotherm model other than the Langmuir model. Both of the n value and the adsorption capacity value suggest that As(V) was preferentially adsorbed onto MFO-C (i.e., a mesoporous akaganeite with low crystallinity in nature), which is in good agreement with conclusions in literature [43,44]. It is noted that the adsorption capacity (q_m = 75.19 mg g^{-1}) of MFO-C was lower than that of akaganeite nanocrystals (i.e., 141.3 mg g^{-1}) reported in literature [45], probably due to its smaller surface area (i.e., 144.7 $m^2\,g^{-1}$) as compared to that of the reported akaganeite nanocrystals (i.e., 330 $m^2\,g^{-1}$).

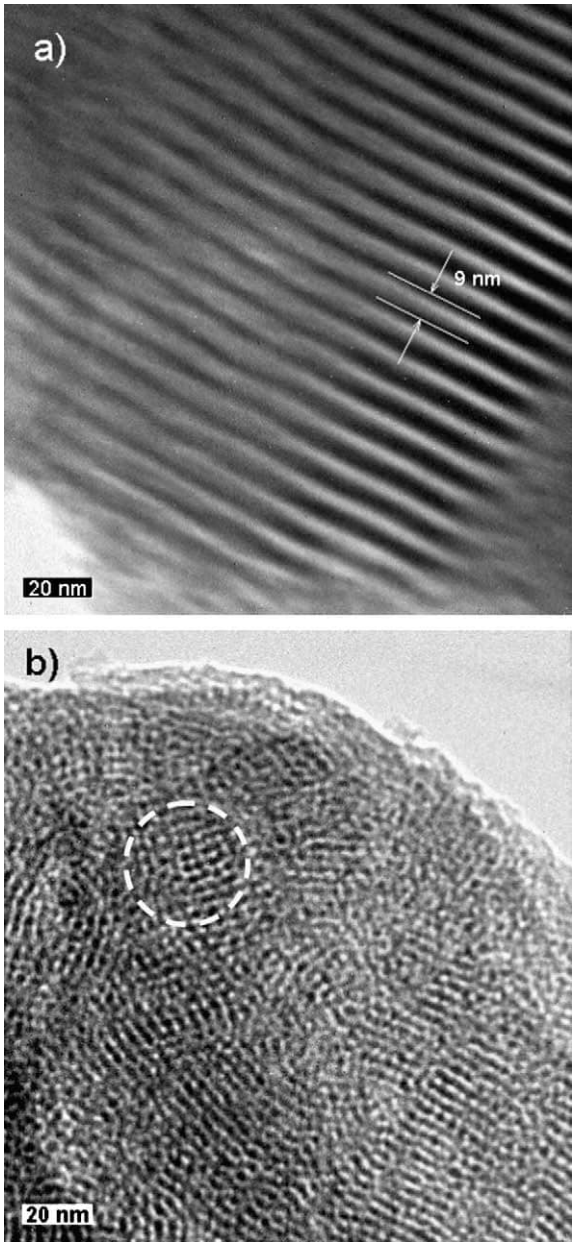

Fig. 6. TEM images of SDS-templated MFOs at $r = 0.5$ using H_2O (a) and EtOH (b) as solvents.

Likewise, the isotherm data of MFO-S were also fitted using both the Langmuir and Freundlich isotherm models with R^2 = 0.981, b = 0.19 L mg^{-1}, q_m = 10.68 mg g^{-1}, and R^2 = 0.993, n = 1.21, K = 3.94, respectively, implying that the Freundlich equation (Eq.(2)) other than the Langmuir equation (Eq.(1)) successfully describes the adsorption behavior of As(V) onto MFO-S at the given

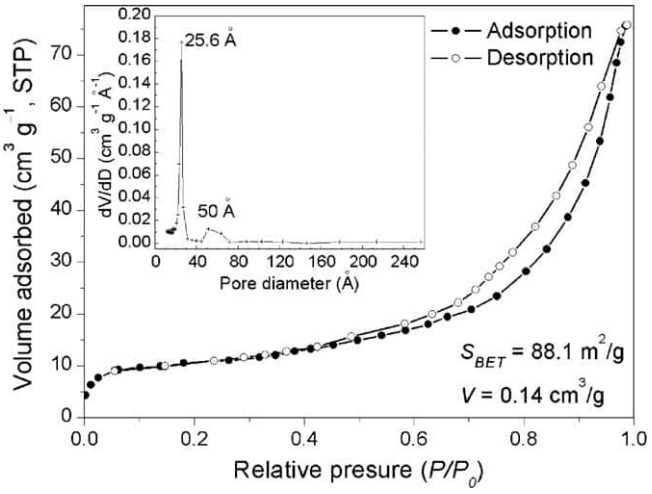

Fig. 7. N_2 adsorption/desorption isotherm of MFO sample synthesized at $r = 0.5$ using EtOH as solvent (inset is the corresponding pore size distribution curve).

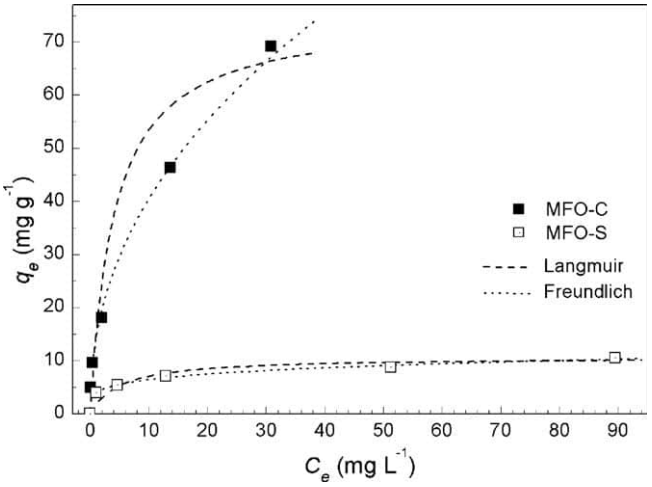

Fig. 8. Adsorption isotherms of arsenate on CTAB-templated MFO (MFO-C, marked with ■) and SDS-templated MFO (MFO-S, marked with □), respectively ($I = 0.01$ M NaCl; pH 7.0 ± 0.1; $T = 298 \pm 1$ K; $t = 24$ h). The equilibrium data fitting to the Langmuir and Freundlich equations were drawn as dash line (- - - -) and dot line (·····), respectively.

range of As(V) concentration. The adsorption capacity of MFO-S (q_m = 10.68 mg g^{-1}) was evidently lower than that of MFO-C, which may arise from not only the difference in mineralogical nature (*cf.* Figs. 1d and 4d), but also and more likely, the distinction in surface area, namely, the surface area of MFO-S (i.e., 80.1 m^2 g^{-1}) was lower than that of MFO-C. It is reported that the mechanism aspect responsible for As(V) adsorption onto ferric oxyhydroxides, especially akaganeite was related to bidentate binuclear comer-sharing between As(V) tetrahedra and adjacent edge-sharing [FeO_6] octahedral [33,46]. In present study, nevertheless, the adsorption mechanism understanding for As(V) onto both MFO-C and MFO-S is under consideration, and it may be uncovered by X-ray adsorption spectrometry in follow-up investigations.

4. Conclusions

Mesostructured ferric oxyhydroxides (MFOs) with worm-like pores were successfully synthesized in the presence of fluoride ions using cetyltrimethylammonium bromide (CTAB) as template. The active role of F^- in improving the mesostructural ordering of MFOs was proved. In the case of sodium dodecylsulfonate (SDS) adopted as template, lamellar mesostructure ferric oxyhydroxides were also easily prepared using either H_2O or EtOH as solvents, and furthermore, the layered mesostructure from the ethanol-solvent system was featured with two different types of lamellar channels as verified by XRD data. It is noted that propanol hampered the formation of mesostructure due to its longer alkyl chain as compared to EtOH. Both of the two typical MFOs (primarily consisted of akaganeite) selected as adsorbent for As(V) removal yielded adsorption isotherms well fitting the Freundlich equation. The typical MFOs exhibited good performance in adsorption of As(V) (i.e., 75.19 mg g^{-1} for MFO-C, 10.68 mg g^{-1} for MFO-S) and could be employed as adsorbent for As(V) removal.

Acknowledgements

This work was partially supported by the Research Funds of State Key Laboratory of Pollution Control and Resource Reuse, the Research Funds of Nanjing University of Information Science and Technology, and the Modern Analysis Center of Nanjing University. The authors thank Bozhi Tian at Harvard University for his helpful discussions.

Appendix A. Supplementary data

Supplementary data associated with this article can be found, in the online version, at doi:10.1016/j.micromeso.2009.03.044. The Supporting Information includes XRD patterns of the CTAB-templated MFOs as a function of pH in the synthetic solution without fluoride ions (Fig. S1) as well as XRD patterns of the SDS-templated MFOs as a function of hydrolysis ratio using PrOH as solvent (Fig. S2).

References

[1] M. Tondel, M. Rahman, A. Magnuson, I.A. Chowdhury, M.H. Faruquee, S.A. Ahmad, Environ. Health Perspect. 107 (1999) 727.
[2] R. Nickson, J. McArthur, W. Burgess, K.M. Ahmed, P. Ravenscroft, M. Rahman, Nature 395 (1998) 338.
[3] A.A. Meharg, M. Rahman, Environ. Sci. Technol. 37 (2003) 229.
[4] S. Dixit, J.G. Hering, Environ. Sci. Technol. 37 (2003) 4182.
[5] T. Pal, P.K. Mukherjee, S. Sengupta, Curr. Sci. 82 (2002) 554.
[6] M. Berg, H.C. Tran, T.C. Nguyen, H.V. Pham, R. Schertenleib, W. Giger, Environ. Sci. Technol. 35 (2001) 2621.
[7] C.H. Tseng, T.Y. Tai, C.K. Chong, C.P. Tseng, M.S. Lai, B.J. Lin, H.Y. Chiou, Y.M. Hsueh, K.H. Hsu, C.J. Chen, Environ. Health Perspect. 108 (2000) 847.
[8] G. Concha, B. Nermell, M. Vahter, Environ. Health Perspect. 106 (1998) 355.
[9] L.C. Roberts, S.J. Hug, T. Ruettimann, M. Billah, A.W. Khan, M.T. Rahman, Environ. Sci. Technol. 38 (2004) 307.
[10] P.L. Smedley, D.G. Kinniburgh, Appl. Geochem. 17 (2002) 517.
[11] G. Sun, Toxicol. Appl. Pharmacol. 198 (2004) 268.
[12] D. Mohan, C.U. Pittman, J. Hazard. Mater. 142 (2007) 1.
[13] USEPA Arsenic Treatment Technologies for Soil, Waste, and Water, EPA-542-R-02-004, Washington, DC, 2002.
[14] Y. Zhang, M. Yang, X.M. Dou, H. He, D.S. Wang, Environ. Sci. Technol. 39 (2005) 7246.
[15] H. Genc-Fuhrman, J.C. Tjell, D. McConchie, Environ. Sci. Technol. 38 (2004) 2428.
[16] B.A. Manning, S.E. Fendorf, S. Goldberg, Environ. Sci. Technol. 32 (1998) 2383.
[17] A.D. Redman, D.L. Macalady, D. Ahmann, Environ. Sci. Technol. 36 (2002) 2889.
[18] A. Jain, K.P. Raven, R.H. Loeppert, Environ. Sci. Technol. 33 (1999) 1179.
[19] E. Lombi, W.W. Wenzel, R.S. Sletten, J. Plant Nutr. Soil Sci. Z. Pflanzenernahr. Bodenkd. 162 (1999) 451.
[20] J.A. Munoz, A. Gonzalo, M. Valiente, Environ. Sci. Technol. 36 (2002) 3405.
[21] Z.M. Gu, B.L. Deng, Environ. Eng. Sci. 24 (2007) 113.
[22] M. Arienzo, P. Adamo, J. Chiarenzelli, M.R. Bianco, A. de Martino, Chemosphere 48 (2002) 1009.
[23] D. Mishra, J. Farrell, Environ. Sci. Technol. 39 (2005) 9689.
[24] Q. Huo, D.I. Margolese, U. Ciesla, P. Feng, T.E. Gier, P. Sieger, R. Leon, P.M. Petroff, F. Schueth, G.D. Stucky, Nature 368 (1994) 317.
[25] F. Schuth, Chem. Mat. 13 (2001) 3184.
[26] D.N. Srivastava, N. Perkas, A. Gedanken, I. Felner, J. Phys. Chem. B 106 (2002) 1878.
[27] Q. Liu, W.M. Zhang, Z.M. Cui, B. Zhang, L.J. Wan, W.G. Song, Micropor. Mesopor. Mat. 100 (2007) 233.

[28] B. Mehendale, R. Shende, S. Subramanian, S. Gangopadhyay, P. Redner, D. Kapoor, S. Nicolich, J. Energ. Mater. 24 (2006) 341.
[29] Z.Y. Yuan, T.Z. Ren, B.L. Su, in: A Selection from the Presentations of the Third Asia–Pacific Congress on Catalysis, Elsevier Science BV, Dalian, PR China, 2003, p. 743.
[30] Y. Wang, L. Yin, A. Gedanken, Ultrason. Sonochem. 9 (2002) 285.
[31] F. Jiao, P.G. Bruce, Angew. Chem. Int. Edit. 43 (2004) 5958.
[32] A.S. Malik, M.J. Duncan, P.G. Bruce, J. Mater. Chem. 13 (2003) 2123.
[33] Y. Izumi, D. Masih, K. Aika, Y. Seida, Micropor. Mesopor. Mat. 94 (2006) 243.
[34] S.H. Tolbert, P. Sieger, G.D. Stucky, S.M.J. Aubin, C.C. Wu, D.N. Hendrickson, J. Am. Chem. Soc. 119 (1997) 8652.
[35] G. Wirnsberger, K. Gatterer, H.P. Fritzer, W. Grogger, B. Pillep, P. Behrens, M.F. Hansen, C.B. Koch, Chem. Mat. 13 (2001) 1453.
[36] F.H.P. Silva, H.O. Pastore, Chem. Commun. (1996) 833.
[37] L.J. Michot, C. Mathieu, E. Bouquet, Comptes Rendus Acad. Sci. Ser. II C 1 (1998) 167.
[38] S.J. Gregg, K.S.W. Sing, Adsorption, Surface Area and Porosity, Academic Press, London, 1982.
[39] C.M. Flynn, Chem. Rev. 84 (1984) 31.
[40] A. Monnier, F. Schuth, Q. Huo, D. Kumar, D. Margolese, R.S. Maxwell, G.D. Stucky, M. Krishnamurty, P. Petroff, A. Firouzi, M. Janicke, B.F. Chmelka, Science 261 (1993) 1299.
[41] E. Prouzet, F. Cot, C. Boissiere, P.J. Kooyman, A. Larbot, J. Mater. Chem. 12 (2002) 1553.
[42] M. Kruk, M. Jaroniec, Chem. Mat. 13 (2001) 3169.
[43] C.M. Hansel, M.J. La Force, S. Fendorf, S. Sutton, Environ. Sci. Technol. 36 (2002) 1988.
[44] H.D. Pedersen, D. Postma, R. Jakobsen, Geochim. Cosmochim. Acta 70 (2006) 4116.
[45] E.A. Deliyanni, D.N. Bakoyannakis, A.I. Zouboulis, K.A. Matis, Chemosphere 50 (2003) 155.
[46] X.J. Guo, Y.H. Du, F.H. Chen, H.S. Park, Y.N. Xie, J. Colloid Interf. Sci. 314 (2007) 427.

Supporting information for:

Synthesis of mesostructured ferric oxyhydroxides templated by alkyl surfactants: Effect of pH, F^- and solvents, and their adsorption isotherms for As(V)

Feihu Li [a, b], Hao Fu [a], Jianping Zhai [a], Qin Li [a]

[a] *State Key Laboratory of Pollution Control & Resource Reuse, and School of the Environment, Nanjing University, Nanjing 210093, China*
[b] *School of Environmental Science & Engineering, Nanjing University of Information Science & Technology, Nanjing 210044, China*

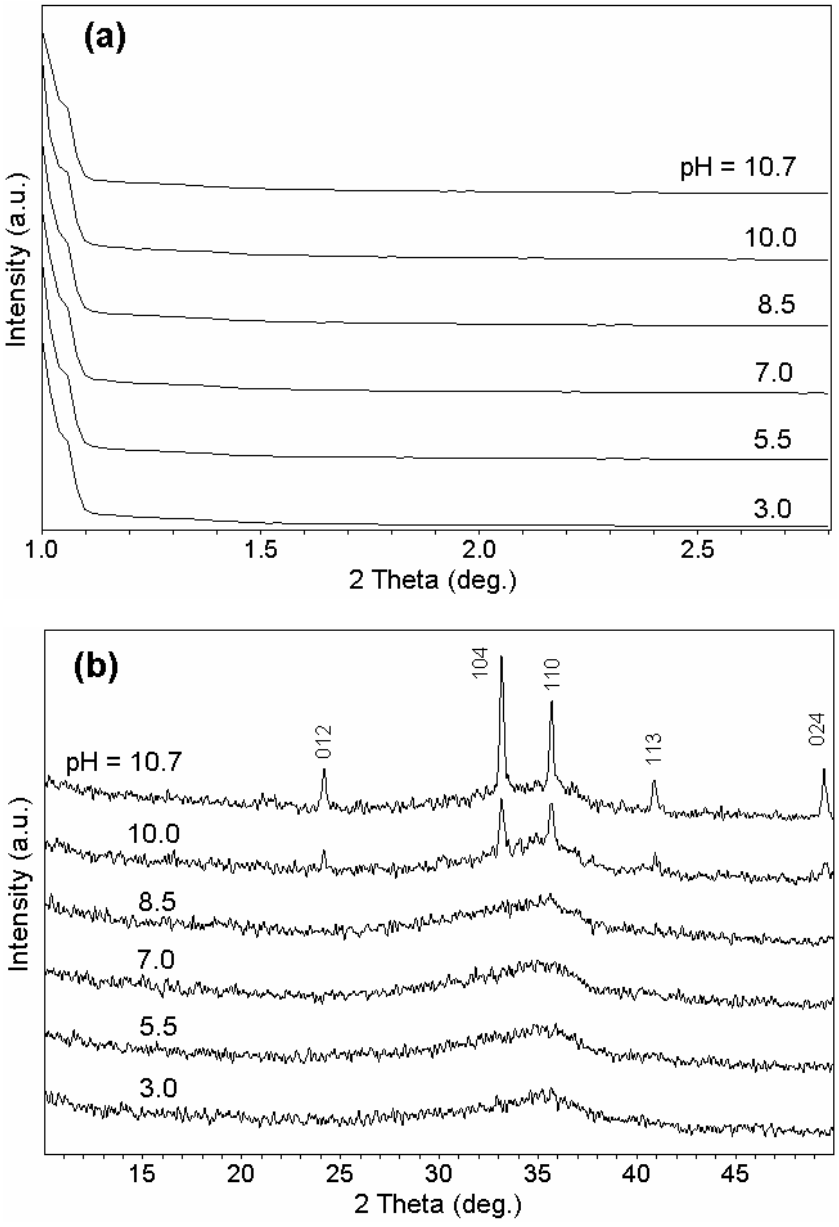

Fig. S1. Small-angle (a) and wide-angle (b) XRD patterns of the CTAB-templated MFOs as a function of pH in the synthetic solution without F^-.

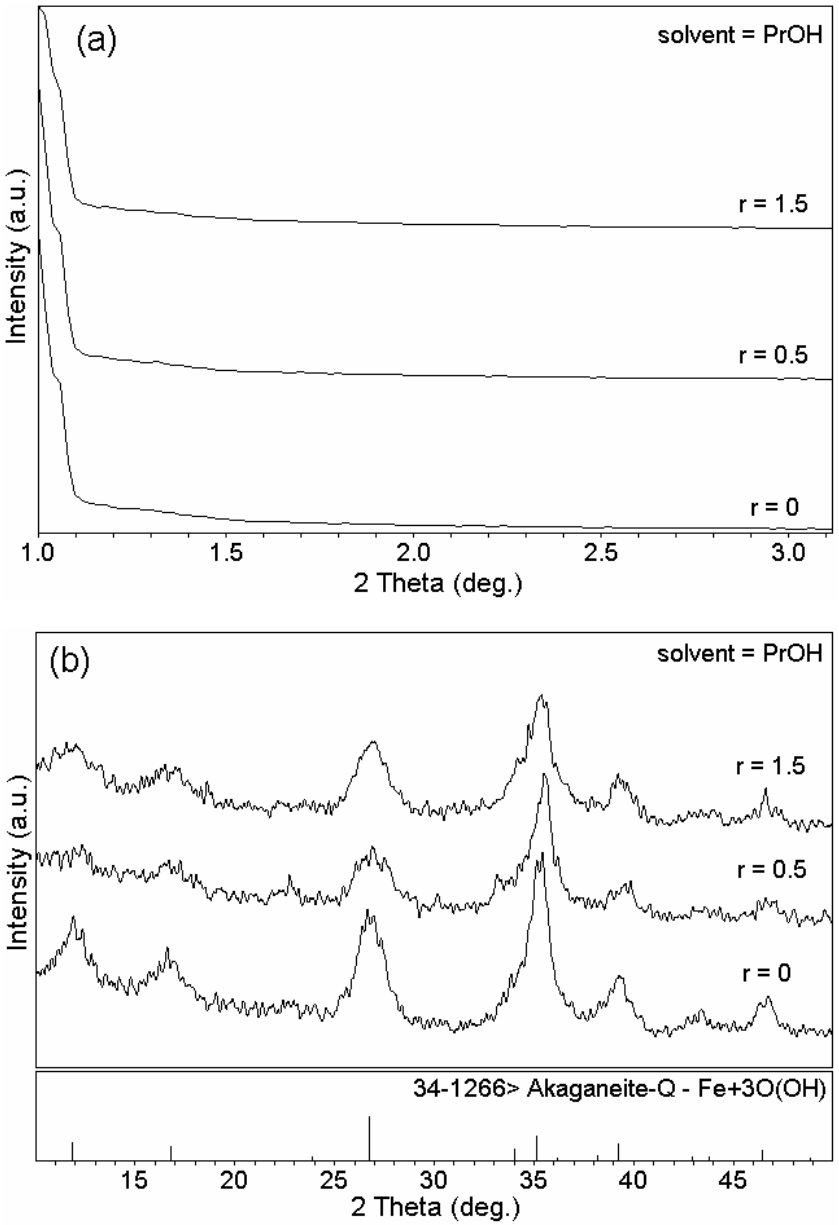

Fig. S2. Small-angle (a) and wide-angle (b) XRD patterns of the SDS-templated MFOs as a function of hydrolysis ratio *r* using PrOH as solvent.